RSC Advances

ROYAL SOCIETY OF CHEMISTRY

www.rsc.org/advances

Effects of Mo/W codoping on the visible-light photocatalytic activity of monoclinic $BiVO_4$ within the GGA+ U framework

Jihua Zhang,[a,b] Mingsen Deng, *,[a,c] Fengzhu Ren[b], Yu Wu[a], Yuanxu Wang, *,[a,b]

[a]Guizhou Provincial Key Laboratory of Computational Nano-Material Science, Guizhou Education University, 115 Gaoxin Road, Guiyang, 550018, China.

[b]Institute for Computational Materials Science, School of Physics and Electronics, Henan University, Kaifeng 475004, China.

[c]Guizhou Synergetic Innovation Center of Scientific Big Data for Advanced Manufacturing Technology, Guizhou Education University, Guiyang, 550018, China.

Email: deng@gznc.edu.cn; wangyx@henu.edu.cn

Abstract: The formation energy, electronic properties, and photocatalytic activity of Mo, W mono-doped and Mo/W codoped $BiVO_4$ were investigated using density functional theory plus U calculations (DFT+U). The calculated formation energies show that both Mo and W atoms prefer to substitute V atoms under the oxygen-rich condition, in agreement with previous experimental results. Mo or W atom doping on V site can form continuum states above conduction band edge of $BiVO_4$, which is advantageous to the photochemical catalysis response. Moreover, we found that the W doped $BiVO_4$ has a smaller band gap than the Mo doped one, and the effect of Mo and W doping on the electronic structure of $BiVO_4$ is different. Mo/W/Mo and W/Mo/W co-doped BiVO4 have smaller formation energies and smaller band gaps than other doping case, which may enhance the optical absorption. Thus, Mo/W/Mo and W/Mo/W co-doped $BiVO_4$ is particularly suitable for visible-light photocatalysis.

1. Introduction

The photocatalytic activity of semiconductors is one of the key factors that limit the quantum efficiency of photocatalysis and must be significantly enhanced to accelerate the photoreaction under light, in particular for visible light. [1, 2] Due to the suitable band gap energy and the chemical stability, $BiVO_4$ is considered as an attractive photocatalyst and has been extensively studied. [3-8] Several different phases of $BiVO_4$ have been observed, such as tetragonal zircon (tz-), tetragonal scheelite (ts-), and monoclinic scheelite (ms-).[9] Among these phases, under visible-light irradiation, ms-$BiVO_4$ has been found to exhibit the highest photocatalytic activity.[10-12] The valence bands (VB) of $BiVO_4$ are composed of hybridized Bi 6*s* and O 2*p* orbitals. The hybridization of the Bi 6*s* and O 2*p* levels leads to a large dispersion of the VB, which favors the mobility of photogenerated holes and is beneficial to the oxidation reaction [13, 14]. In addition, the effective masses of the electron and the hole in $BiVO_4$ were predicted to be much lighter than those in other semiconductors (e.g., TiO_2 and In_2O_3). [15, 16]

However, the typical efficiency of pure $BiVO_4$ for water oxidation is not impressive, due to excessive electron–hole recombination and poor water oxidation kinetics[17-19]. These deficiencies thus greatly limit the practical applications of $BiVO_4$. Many attempts have been made to enhance the photocatalytic and photoelectrochemical (PEC) activity of $BiVO_4$ by controlling the morphology, [20, 21] forming composite structures or heterojunctions, [22-24] doping or composition tuning, [25-27] and coupling with oxygen evolution catalysts (OECs). [28] Among these methods, ion doping is a simple approach and one of the most effective methods. [29] Using a modified metal-organic decomposition method, Parmar *et al.* prepared $BiVO_4$ doped with various metal ions and observed that only Mo^{6+} or W^{6+} doping enhanced the water photo-oxidation activity.[30] For water oxidation or organic compound degradation, Mo-doped $BiVO_4$ was remarkably enhanced[31]. Recently, Abdi *et al.* [32] demonstrated that the carrier-separation efficiencies of W-doped $BiVO_4$ photoanode can achieve to 80%. More importantly, instead of single element-doping, co-doping with W and Mo was found to further improve the photoelectrochemical (PEC)

performance of $BiVO_4$. [33, 34] The carrier density of the Mo/W co-doped $BiVO_4$ sample was demonstrated to be twice that of the W-doped sample.

For doped $BiVO_4$, the impurities can be at either substitutional Bi or V sites[8, 35, 36]. However, the existing forms of Mo and W atoms in doped $BiVO_4$ are often debated. It is expected that the mechanism for Mo impurity incorporation could be different from that for W. Some of the incorporated impurities may contribute to catalytic activity, whereas others may simply affect the crystal growth or alter the formation of defects and subsequently the doping properties. To achieve the optimal performance of Mo/W co-doped $BiVO_4$, it is fundamentally important to identify the forms of the defects that are potential shallow donors or are harmful to the PEC response. It is also essential to determine the growth conditions for the formation of desirable defects and the suppression of harmful defects.

Herein, we systematically investigated the geometry structures, formation energies, and electronic properties of the Mo, W mono-doped and Mo/W codoped $BiVO_4$. The result of our investigation enables us to determine the most stable model for Mo/W co-doped $BiVO_4$. The origin of visible-light absorption and photoactive enhancement for the Mo/W co-doped $BiVO_4$ were revealed by exploring the effects of the changes in band gaps, distributions of the impurity states, and energies of the band edges.

2. Models and methods

2.1 Computational details

All geometric optimizations and electronic structure calculations were performed using spin-polarized density functional theory (DFT), as implemented in the Vienna ab initio Simulation Package (VASP) [37, 38]. The project-augmented wave method for core valence interactions and the generalized gradient approximation (GGA) of the Perdew–Burke–Erzerhof (PBE) form for the exchange-correlation function were used. [39-42] For selected systems, we also used DFT (GGA)+U within Dudarev's approach. [43] We applied the U = 2.7 eV[44] for the V 3*d* states in $BiVO_4$. For the Mo/W co-doped $BiVO_4$ cases, U = 2.3 eV for Mo 4*d* and U = 2.1 eV for W 5*d* were chosen, according to Ref [44]. Note that 4*d*- and 5*d*-valence orbitals are generally less spatially localized

than 3*d*-valence orbitals, resulting in smaller U values. Although the properties of doped $BiVO_4$ can be affected by the choice of U, these DFT+U calculations should be appropriate to draw reasonable conclusions. In fact, the hybrid exchange functional (HSE06)[45] has previously been shown to be better at accurately predicting the structure and band gap of $BiVO_4$ compared to the standard DFT functional[46-48]. However, the HSE06 calculations for doped $BiVO_4$ are restricted by our computational resources. From Section 3, we will see that the calculated band gap of pure $BiVO_4$ using the GGA+U method is 2.3 eV, which is in good agreement with the experimental value of 2.5 eV[49]. Therefore, instead of HSE06, the GGA+U method is used in the current calculations. The Kohn-Sham one-electron states were expanded in a plane wave basis set up to 500 eV. For pure BiVO4 and Mo/W co-doped $BiVO_4$, the Monkhorst–Pack k-point mesh of 5 × 3 × 7 and 3 × 3 × 3 was used to perform geometry optimizations, and 10 × 6 × 7 and 6 × 6 × 6 k-point mesh was used for the electronic structure calculations [50], respectively. At the end of the structural optimizations process, the residual Hellman–Feynman forces on each ion became less than 0.03 $eVÅ^{-1}$. The criterion for the total energy is set as 1×10^{-5} eV. The density of states (DOS) was calculated using the tetrahedron method with Blöchl corrections. Moreover, the accuracy of the calculations was tested by increasing the cutoff energy and the number of k points, and negligible changes in the energy and geometry structure were observed. After finishing the geometry optimization, the band structure and projected density of state (PDOS) of the pure, Mo, W mono-doped, and Mo/W co-doped $BiVO_4$ were calculated.

2.2 Doped configuration

Both I2/b and C2/c space groups are commonly used to describe the monoclinic scheelite structure of $BiVO_4$[8]. The space group, I2/b, with which the monoclinic scheelite structure of $BiVO_4$ was originally reported is a non-standard space group[51]. It can be converted to a standard space group, C2/c, which is used in some recent studies of BiVO4[15, 23]. Here we choose I2/b space groups, this because which has the advantage of easily showing its structural relationship to the tetragonal scheelite structure[8]. The monoclinic $BiVO_4$ structure was determined through careful volume

optimization and atomic position relaxation with a primitive unit cell (consisting of two $BiVO_4$ units). By optimizing the pure ms-$BiVO_4$ structure, we obtained the following lattice parameters: a = 5.1507 Å, b = 5.0958 Å, c = 11.6067 Å, and γ = 90.2416° (space group I2/b). These lattice parameters are in good agreement with experimental values [51]: a =5.1935 Å, b = 5.0898 Å, c = 11.6972 Å, and γ = 90.3871°. These results indicate that our calculation methods can give reasonably good values. For doping structures, as shown in Fig. 1, the 2 × 2 × 1 supercell (containing 16 bismuth or vanadium atoms and 64 oxygen atoms) of monoclinic $BiVO_4$ was simultaneously doped with one Mo atom and one W atom. The impurity atoms were introduced into the supercell with the modes of Mo_{Bi} (Mo atom substituting for the lattice Bi atom), Mo_V (Mo atom substituting for the lattice V atom), W_{Bi} (W atom substituting for the lattice Bi atom), and W_V (W atom substituting for the lattice V atom), resulting in four different modes of Mo/W co-doped monoclinic $BiVO_4$ models (Mo_VW_V-$BiVO_4$, Mo_VW_{Bi}-$BiVO_4$, $Mo_{Bi}W_{Bi}$-$BiVO_4$, and $Mo_{Bi}W_V$-$BiVO_4$). To further determine the stable mono-doped configurations, we constructed 16 possible mono-doped systems for Mo_{Bi}, Mo_V, W_{Bi}, and W_V and calculated their total energies. It is found that Mo_{Bi} at (0.75, 0.625, 0.8665), Mo_V at (0.75, 0.375, 0.63), W_{Bi} at (0.75, 0.875, 0.1335), and W_V at (0.5, 0.875, 0.87) positions have lower total energy than other positions. For $Mo_{Bi}W_V$-$BiVO_4$ and $Mo_{Bi}W_{Bi}$-$BiVO_4$, we fixed Mo_{Bi} at the (0.75, 0.625, 0.8665) position, constructed 15 and 16 possible co-doped systems for W_{Bi}, and W_V, respectively, and then calculated their total energies. It is found that W_{Bi} at (0.75, 0.875, 0.1335) and W_V at (0.5, 0.875, 0.87) (seen in Fig. 2(j)) have lower total energy than at the other positions. Similarly, for Mo_VW_V-$BiVO_4$ and Mo_VW_{Bi}-$BiVO_4$, we fixed Mo_V at the position of (0.75, 0.375, 0.63) and then constructed 16 and 15 possible co-doped systems for W_{Bi}, and W_V, respectively. The calculated total energies demonstrate that W_{Bi} at (0, 0.125, 0.6335) and W_V at (0.25, 0.375, 0.63) (seen in Fig. 2(k)) have lower total energy than at the other positions. In the following, we will only focus on the configuration with the lowest energy for mono-doped or co-doped systems. Furthermore, to compare the electronic properties of Mo/W co-doped $BiVO_4$ with those of mono-doped $BiVO_4$, the supercell models of Mo_{Bi}-$BiVO_4$, Mo_v-$BiVO_4$,

W_{Bi}-$BiVO_4$ and W_v-$BiVO_4$ were also calculated.

Experimentally, the doping amounts of Mo and W are often not equal[34]. To explore its possible mechanism, we increased the Mo or W doping concentration further and considered Mo/W/Mo (atomic number ratio of Mo and W is 2:1) and W/Mo/W (atomic number ratio of Mo and W is 1:2) co-doped $BiVO_4$, respectively. Moreover, the Mo, W dopant concentrations (mole ratio) in our calculations can be achieved 3.125%. This mole ratio could be comparable to those in experiments, which are 6%[34] or 8%[33] respectively. From Section 3, we will see that when Mo doped on the Bi lattice site, it might be harmful for PEC efficiency. In this case, we only focus on Mo or W doped on the V lattice site. We fixed Mo_V at the position of (0.75, 0.375, 0.63) and W_V at the position of (0.25, 0.375, 0.63) and then constructed 14 and 14 possible co-doped systems for Mo_v, and W_V, respectively. The calculated total energies show that Mo_v at the position of (0.5, 0.375, 0.87) (seen in Fig. 3(c)) and W_V at the position of (0.5, 0.375, 0.87) (seen in Fig. 3(d)) have lower total energy than the other positions. In the following, we will only focus on the configurations with the lowest energy for 1:2 $BiVO_4$ co-doped systems.

2.3. Formation energies

To compare the relative feasibilities of the doping modes above, the formation energies (E_{form}) for Mo/W co-doped as well as for mono-doped $BiVO_4$ were calculated; the formation energy is defined by the following expression:

$$E_{form} = E_{doped} - E_{pure} - p\times\mu_{Mo} - q\times\mu_{W} + x\times\mu_{Bi} + y\times\mu_{V},$$

where E_{doped} is the total energy of the Mo,W mono-doped or Mo/W co-doped $BiVO_4$ supercell and E_{pure} is the total energy of the pure $BiVO_4$ supercell[52, 53]. μ_{Mo}, μ_{W}, μ_{Bi} and μ_{V} are the chemical potentials of Mo, W, Bi, and V atoms, respectively. The coefficients p and q (equal to 0, 1, or 2) represent the numbers of Mo and W, respectively, and x and y (equal to 0, 1, or 2) represent the numbers of Bi and V atoms, respectively. Note that E_{form} is not fixed but depends on the growth conditions. By adjusting the O_2 pressure, the growth conditions can be changed from O-rich to O-poor. The relationships between oxygen and the chemical potentials of Mo, W, Bi, and V atoms are as follows:

$$\mu_{Mo} + 3\mu_O = \mu(MoO_3), \quad (2)$$

$$\mu_W + 3\mu_O = \mu(WO_3), \quad (3)$$

$$2\mu_{Bi} + 3\mu_O = \mu(Bi_2O_3), \quad (4)$$

$$\mu_V + 2\mu_O = \mu(VO_2). \quad (5)$$

Under O-rich growth conditions, μ_O is determined by the ground-state energy of the O_2 molecule ($\mu_O = \mu_O(O_2)/2$). Thus, the chemical potentials of Mo, W, Bi, and V atoms can be obtained from Eqs. (2), (3), (4), and (5), respectively. While under extreme reducing conditions, μ_V is determined by the ground-state energy of bulk V ($\mu_V = \mu_{bulk}/n$, n is the number of V atom in the bulk V). The value of μ_{Bi} determined by the ground-state energy of bulk Bi ($\mu_{Bi} = \mu_{bulk}/n$, n is the number of Bi atom in the bulk Bi) does not change[29]. According to Eq. (5), μ_O is calculated. Then, μ_{Mo} and μ_W can be obtained from Eqs. (2) and (3), respectively. Considering that the calculated μ_O in O-rich growth conditions is larger by 3 eV than that in O-poor growth conditions, μ_O is transformed into the form of $\mu_O = 1/2 \times \mu_O(O_2) + \mu'_O$, where $\mu'_O = -3$ eV corresponds to O-poor growth conditions and $\mu'_O = 0$ eV corresponds to O-rich growth conditions (condensation oxygen). According to Eqs. (1)–(5), E_{form} can thus be calculated from the following expression:

$$E_{form} = E_{doped} - E_{pure} - p\times\mu(MoO_3) - q\times\mu(WO_3) + (x/2)\times\mu(Bi_2O_3) + y\times\mu(VO_2) + (3p/2+3q/2-3x/2-y)\times\mu(O_2) + (3p+3q-3x/2-2y)\times\mu'_O \quad (6)$$

Table 1 lists the formation energies of doped supercells under the O-poor and O-rich growth conditions. Under the oxygen-poor condition, the doping processes of Mo,W mono-doped and Mo/W co-doped $BiVO_4$ with positive E_{form} become non-spontaneous reactions, implying that the oxygen-poor condition inhibits the doping process of Mo,W mono-doped and Mo/W co-doped $BiVO_4$. In particular, under oxygen-rich growth conditions, Mo_vW_V-$BiVO_4$ is the most stable system due to its lowest formation energy (-0.79 eV), and the next most stable ones are Mo_V-$BiVO_4$ (-0.65 eV) and W_v-$BiVO_4$ (-0.15 eV). These results confirm that the Mo and W atoms prefer to substitute V atom under the oxygen-rich condition, consistent with the experimental results[54]. This result also indicates that the chosen parameters in the calculations are quite reasonable.

It is intriguing to see in Table 1 that under oxygen-rich growth conditions, the Mo/W/Mo- $BiVO_4$ is the most stable system due to its lowest formation energy (-1.38 eV), indicating that Mo/W/Mo co-doping could be easier to obtain experimentally than the other combinations (e.g., Mo_v-$BiVO_4$, Mo_VW_V-$BiVO_4$, and W_v-$BiVO_4$). The formation energy of W/Mo/W-$BiVO_4$ is smaller than that of W_VMo_V (-0.79 eV) and smaller than that of W_V (-0.15 eV), which results from the better ion size matching of Mo and V.

3. Results and discussion

The E_{form} of Mo_{Bi}-$BiVO_4$ and $Mo_{Bi}W_V$-$BiVO_4$ is 0.81eV and 0.53eV, respectively, which is close to that of Mo_V-$BiVO_4$ (-0.65 eV) and W_v-$BiVO_4$ (-0.15 eV). Therefore, to compare Mo or W atom doping on V site $BiVO_4$, the electronic properties of the Mo_{Bi}-$BiVO_4$ and $Mo_{Bi}W_V$-$BiVO_4$ are also calculated. To clarify the origination of enhanced visible-light photocatalytic activity of Mo or W doped $BiVO_4$, the band structures, the projected density of states (PDOS), and the band decomposed charge densities for the pure-$BiVO_4$, W_V-$BiVO_4$, Mo_{Bi}-$BiVO_4$, Mo_v-$BiVO_4$, $Mo_{Bi}W_V$-$BiVO_4$, and Mo_VW_V-$BiVO_4$ were calculated using the DFT+U method and were plotted in Fig. 2 (a-k). Comparing Fig2 (a - f) and Fig. S1 - S4 (Fig. S1 - S4 in Supplemental Material which geometrical structure is the same as Fig. 2), we found that the band gap increases with DFT+U method, while the shape of the electronic band structure remains nearly unchanged with respect to the normal DFT calculations.

As shown in Fig. 2(a), the pure $BiVO_4$ is an indirect band gap semiconductor, which is consistent with the experimental result[49]. The band gap of $BiVO_4$ increases to 2.3 eV from DFT+U calculations, which is close to the experimental result (2.5 eV) and is consistent with the previous theoretical study[33] . This result indicates that the chosen U value is sufficiently large for V 3*d*; in the literature, the commonly applied U values for V 3*d* are in the range of 2 to 4 eV[44, 55]. The conduction bands of pure $BiVO_4$ are mainly composed of O 2*p* and V 3*d* states, while the valence bands are composed of O 2*p* states. It is noted that band gaps from the DFT+U method are not directly comparable to experiment. However, we mainly focus on the change of the band gap after Mo, W mono-doped and Mo/W co-doping, which can be well

described by DFT+U method in present work.

In the cases of W_V-$BiVO_4$, Mo_{Bi}-$BiVO_4$, Mo_v-$BiVO_4$, $Mo_{Bi}W_V$-$BiVO_4$, and Mo_VW_V-$BiVO_4$ (see Figs. 2 b-f), in comparison with pure $BiVO_4$, one can clearly see that (1) for Mo_V and/or W_V, the Mo 4*d* state tends to be localized in the bottom of the conduction bands, which leads to the extending of the conduction bands [see Fig 2(b)(f)], while the W 5*d* state goes deeply into the conduction bands, which strongly affects the V 3*d* state [see Fig 2(c)(f)]; (2) all of these doping are potential donors for realizing good *n*-type conductivities; and (3) doping with Mo, W leads to narrowing of the band gap, and W doped system shows a smaller gap than Mo doped one.

For the W_V-$BiVO_4$ (seen in Fig. 2b), there is no isolated state in the band gap, and the W 5*d* impurity states appear in the same energy region with V 3*d* states, impling a hybridization between the W 5*d* and V 3*d* states. There is one main peak of the V 3*d* spin-down state near E_F (-0.05 V). The corresponding band decomposed charge density isosurface (see Fig. 2g) reveals that the charge density spreads over four V atoms. The conduction bands are mainly composed of V 3*d* states, while the valence bands mainly consisted of O 2*p* states. Thus, the valence bands extends towards the conduction bands and the eigenvalue gap (E_g), and the distance between O 2*p* states and V 3*d* states around E_F (see Fig 2), is 2.23 eV, which is close to that of pure $BiVO_4$ (2.3 eV). Therefore, W doping weakly changes the band gap of $BiVO_4$, which is in agreement with the experimental result [33].

As shown in Figs. 2(c) and 2(e), for Mo_{Bi}-$BiVO_4$ and $Mo_{Bi}W_V$-$BiVO_4$, Mo doping on the Bi lattice site will induce Mo 4d impurity states located in the band gap. These impurity states can easily trap the carriers and lead to the reduction in carrier mobility and conversion efficiency,[56] which is a harmful for the application of Mo_{Bi}-$BiVO_4$ and $Mo_{Bi}W_V$-$BiVO_4$ in the photoelectrochemical conversion of solar energy. Thus, although Mo_{Bi}-$BiVO_4$ and $Mo_{Bi}W_V$-$BiVO_4$ systems have a significant reduction in the photo transition energy, they are not so suitable for enhancing the photocatalytic activity in the visible light region. In practice, to increase the PEC efficiency, we should control the growth conditions to avoid the formation of Mo_{Bi}-$BiVO_4$ and $Mo_{Bi}W_V$-$BiVO_4$. For Mo_{Bi}-$BiVO_4$, the value of E_g is 2.27 eV, which

is close to that of pure $BiVO_4$ (2.3 eV). This is consistent with the previous results[33, 57]. While for $Mo_{Bi}W_V$-$BiVO_4$, the value of E_g is decreased to 2.15 eV. This result indicates that the influence of W doping on E_g is stronger than that of Mo doping. The corresponding band decomposed charge density isosurface (see Fig. 2h and 2j) reveals that the charge density spreads over the Mo/O atoms and V atoms.

As shown in Fig. 2 (d), a significant perturbation occurs at the conduction band minimum (CBM) and the Fermi level is above the conduction band. In addition, the conduction band edge is still determined by the V 3d state. The E_g is decreased to 2.23 eV. The corresponding band decomposed charge density isosurface (see Fig. 2i) reveals that the charge density spreads over the Mo atom. As shown in Fig. 2f, the band edge shifts of the Mo_VW_V-$BiVO_4$ exhibit the same chemical trends as those observed in both the Mo_v-$BiVO_4$ and W_v-$BiVO_4$. Simultaneously, the value of E_g is decreased to 2.08 eV. The band decomposed charge density isosurface (see Fig. 2k) reveals that the charge density spreads over the Mo atom and five V atoms.

To further investigate the effect of doping on the band gap, the Mo/W/Mo-$BiVO_4$ and W/Mo/W-$BiVO_4$ is considered. Figure 3 (a-d) shows the band structures, PDOS plots, and the band decomposed charge density within the energy range of –0.5 to 0 eV (isosurface values 0.01 e/Å^3) for Mo/W/Mo-$BiVO_4$ and W/Mo/W-$BiVO_4$. As shown in Fig 3, with increasing Mo or W doping, the impurity state continuously moves toward the valence bands by approximately 0.2 eV. The corresponding band decomposed charge density isosurface for Mo/W/Mo-$BiVO_4$ indicates that the charge density spreads over the two Mo atoms and the seven V atoms, while for W/Mo/W-$BiVO_4$, the impurity state comes from different V atoms. In this case, continuum states above the CB edge are formed rather than isolated states, and thus leads to a real band gap narrowing and consequently a redshift of the optical absorption edge[58], which is favorable for enhancing the lifetimes of photoexcited carriers[56, 59]. This enhancement is similar to the phenomenon in Nb/C/Nb co-doped TiO_2 [56] and N/H-codoped TiO_2[58]. Compared with Mo_VW_V-$BiVO_4$, the values of Eg of Mo/W/Mo-$BiVO_4$ and W/Mo/W-$BiVO_4$ are reduced to 1.80 eV and 1.78 eV, respectively, which can enhance the absorptions of visible light.

Characteristic charge redistribution behavior can be obtained by calculating the

charge density difference of the Mo, W mono-doped and Mo/W co-doped $BiVO_4$ before and after the charge transfer. Fig. 4 shows the calculated charge density difference of W_VMo_{Bi}, W_VMo_V, Mo/W/Mo, and W/Mo/W-$BiVO_4$, co-doped $BiVO_4$. As observed from Fig. 4 (a - d) , the charge redistribution is dominantly restricted on Mo/W and O. The amount of the charge transfer of Mo_{Bi} is less than W_V and Mo_V, which is consistent with Mo, W mono-doped $BiVO_4$ (Fig. S5 in the Supplementary Material). In the case of W_V and Mo_V, substantial charge accumulates in the region between the W_V/Mo_V and O atoms. This demonstrates that the bonding between the Mo/W and O atoms is characterized by covalent behavior.

The conduction band and valence band potentials of a semiconductor affect its photocatalytic activity[1]. Based on the Mulliken electronegativity theory[60], the conduction band potentials at the point of zero charge of a semiconductor could be predicted by

$$E_{CB} = \chi - E^c - 0.5E_g, \quad (8)$$

E_{CB}, E_g and χ are the conduction band potential, band-gap energy and absolute electronegativity of a semiconductor, respectively. E^c is the energy of the free electron in the hydrogen scale (approximately 4.5 eV)[61]. The valence band potential could be calculated from $E_{VB} = E_{CB} - E_g$. The χ value for $BiVO_4$ is 6.04 eV [62]. The Mulliken electronegativity of V, Mo, and W are 3.6, 3.9[63], and 4.4eV[64]. This indicates that Mo and/or W doping very weakly changes the χ value of the doped system. Thus, the E_{CB} of doped systems are almost equal to that of the pure which is consistent with the previous computational results[65]. It means that the driving force required for reduction process almost unchanged. Correspondingly, for the smaller band gap, E_{VB} of doped systems are smaller than that of pure, and thus oxidation processes is lowered in these system.

4. Conclusions

We have carefully examined the formation energy, electronic property, and photocatalytic activity of the Mo, W mono-doped and Mo/W codoped $BiVO_4$ using DFT+U calculations. Much important structure information has been obtained, which will provide useful guidelines for the growth of crystals. We found that under oxygen-rich conditions, the Mo and W atoms prefer to substitute V atom, but the doping of Mo gives a more stable structure. The electronic structure of the

mono-doped is very different, resulting in very different optical absorption behavior. The Mo/W/Mo and W/Mo/W co-doping cases are found to enhance optical absorption due to their reduced band gap compared with the undoped case. The Mo/W/Mo and W/Mo/W co-doped $BiVO_4$ can be considered as good candidates for visible-light photocatalysis in practical applications.

Acknowledgments

This work was supported by the National Natural Science Foundation of China (nos. 11547011, 51371076, 21203037, and 11264005), the Program for Innovative Research Team in the University of Henan Province (nos. 13IRTSTHN017), the Construction Project for Guizhou Provincial Key Laboratories (no. ZJ[2013]4009), the Natural Science Foundation of Guizhou Province (nos. QKH-J[2010]2144, J[2011]2097), and the Guizhou Provincial High-Performance Computing Center of Condensed Materials and Molecular Simulation, the Program for Innovative Research Team of Guizhou Province (No. QKTD[2014]4021). J. H. Z. acknowledges the scientific research fund of GPED (nos. 2114118006zx, QJTD[2013]16) and the GZNC startup package (no. 13BS027). M. S. D acknowledges the support by the Excellent Youth Scientific and Technological Talents of Guizhou Province (no. QKH-RZ[2013]01).

References

1. A. L. Linsebigler, G. Lu and J. T. Yates, *Chem. Rev.*, 1995, 95, 735-758.
2. R. Li, J. Hu, M. Deng, H. Wang, X. Wang, Y. Hu, H. L. Jiang, J. Jiang, Q. Zhang, Y. Xie and Y. Xiong, *Adv. Mater.*, 2014, 26, 4783-4788.
3. A. Kudo, K. Omori and H. Kato, *J. Am. Chem. Soc.*, 1999, 121, 11459-11467.
4. A. Kudo, K. Omori and H. Kato, *J. Am. Chem. Soc.*, 1999, 121, 11459-11467.
5. A. Kudo, K. Ueda, H. Kato and I. Mikami, *Catal. Lett.*, 1998, 53, 229-230.
6. N. Aiga, Q. Jia, K. Watanabe, A. Kudo, T. Sugimoto and Y. Matsumoto, *J. Phys. Chem. C*, 2013, 117, 9881-9886.
7. H. W. Jeong, T. H. Jeon, J. S. Jang, W. Choi and H. Park, *J. Phys. Chem. C*, 2013, 117, 9104-9112.
8. Y. Park, K. J. McDonald and K. S. Choi, *Chem. Soc. Rev.*, 2013, 42, 2321-2337.
9. J. D. Bierlein and A. W. Sleight, *Solid State Commun.*, 1975, 16, 69-70.
10. S. Tokunaga, H. Kato and A. Kudo, *Chem. Mater.*, 2001, 13, 4624-4628.
11. J. Yu and A. Kudo, *Adv. Funct. Mater.*, 2006, 16, 2163-2169.
12. H. Yoon, M. G. Mali, J. Y. Choi, M. W. Kim, S. K. Choi, H. Park, S. S. Al-Deyab, M. T. Swihart, A. L. Yarin and S. S. Yoon, *Langmuir*, 2015, 31, 3727-3737.
13. M. Oshikiri, M. Boero, J. Ye, Z. Zou and G. Kido, *J. Chem. Phys.*, 2002, 117, 7313-7318.
14. L. Zhang, D. Chen and X. Jiao, *J. Phys. Chem. B*, 2006, 110, 2668-2673.
15. Z. Zhao, Z. Li and Z. Zou, *Phys. Chem. Chem. Phys.*, 2011, 13, 4746-4753.
16. A. Walsh, Y. Yan, M. N. Huda, M. M. Al-Jassim and S.-H. Wei, *Chem. Mater.*, 2009, 21, 547-551.
17. F. F. Abdi, T. J. Savenije, M. M. May, B. Dam and R. van de Krol, *J. Phys. Chem. Lett.*, 2013, 4, 2752-2757.
18. J. Ravensbergen, F. F. Abdi, J. H. van Santen, R. N. Frese, B. Dam, R. van de Krol and J. T. M. Kennis, *J. Phys. Chem. C*, 2014, 118, 27793-27800.
19. Y. Ma, S. R. Pendlebury, A. Reynal, F. Le Formal and J. R. Durrant, *Chemical Science*, 2014, 5, 2964.
20. W. Luo, Z. Wang, L. Wan, Z. Li, T. Yu and Z. Zou, *J. Phys. D: Appl. Phys.*, 2010, 43, 405402.
21. G. Xi and J. Ye, *Chem. Commun.*, 2010, 46, 1893-1895.
22. J. Su, L. Guo, N. Bao and C. A. Grimes, *Nano Lett.*, 2011, 11, 1928-1933.
23. J. Zhang, F. Ren, M. Deng and Y. Wang, *Phys. Chem. Chem. Phys.*, 2015, 17, 10218-10226.
24. Y. Yang, J. Wang, J. Zhao, B. A. Nail, X. Yuan, Y. Guo and F. E. Osterloh, *ACS Appl. Mater. Interfaces*, 2015, 7, 5959-5964.
25. L. Chen, F. M. Toma, J. K. Cooper, A. Lyon, Y. Lin, I. D. Sharp and J. W. Ager, *ChemSusChem*, 2015, 8, 1066-1071.
26. M. Wang, H. Zheng, J. Liu, D. Dong, Y. Che and C. Yang, *Mater. Sci. Semicond. Process.*, 2015, 30, 307-313.
27. D. K. Zhong, S. Choi and D. R. Gamelin, *J. Am. Chem. Soc.*, 2011, 133,

18370-18377.
28. T. H. Jeon, W. Choi and H. Park, *Phys. Chem. Chem. Phys.*, 2011, 13, 21392-21401.
29. Z. Zhao, W. Luo, Z. Li and Z. Zou, *Phys. Lett. A*, 2010, 374, 4919-4927.
30. K. P. Parmar, H. J. Kang, A. Bist, P. Dua, J. S. Jang and J. S. Lee, *ChemSusChem*, 2012, 5, 1926-1934.
31. W. Yao, H. Iwai and J. Ye, *Dalton trans.*, 2008, DOI: 10.1039/b713338c, 1426-1430.
32. F. F. Abdi, L. Han, A. H. M. Smets, M. Zeman, B. Dam and R. van de Krol, *Nat. Commun.*, 2013, 4, 2195.
33. H. S. Park, K. E. Kweon, H. Ye, E. Paek, G. S. Hwang and A. J. Bard, *J. Phys. Chem. C*, 2011, 115, 17870-17879.
34. S. P. Berglund, A. J. Rettie, S. Hoang and C. B. Mullins, *Phys. Chem. Chem. Phys.*, 2012, 14, 7065–7075.
35. B. Zhou, X. Zhao, H. Liu, J. Qu and C. P. Huang, *Sep. Purif. Technol.*, 2011, 77, 275-282.
36. W.-J. Yin, S.-H. Wei, M. M. Al-Jassim, J. Turner and Y. Yan, *Phys. Rev. B*, 2011, 83, 155102.
37. G. Kresse and J. Furthmüller, *Phys. Rev. B*, 1996, 54, 11169-11186.
38. G. Kresse and J. Furthmüller, *Comp. Mater. Sci.*, 1996, 6, 15-50.
39. G. Kresse and D. Joubert, *Phys. Rev. B*, 1999, 59, 1758-1775.
40. P. E. Blöchl, *Phys. Rev. B*, 1994, 49, 16223-16233.
41. J. P. Perdew and Y. Wang, *Phys. Rev. B*, 1992, 45, 13244-13249.
42. J. P. Perdew, K. Burke and M. Ernzerhof, *Phys. Rev. Lett.*, 1996, 77, 3865-3868.
43. S. L. Dudarev, S. Y. Savrasov, C. J. Humphreys and A. P. Sutton, *Phys. Rev. B*, 1998, 57, 1505-1509.
44. I. V. Solovyev and P. H. Dederichs, *Phys. Rev. B*, 1994, 50, 16861-16871.
45. J. Heyd, G. E. Scuseria and M. Ernzerhof, *J. Chem. Phys.*, 2006, 124, 219906.
46. S. K. Pilli, T. G. Deutsch, T. E. Furtak, J. A. Turner, L. D. Brown and A. M. Herring, *Phys. Chem. Chem. Phys.*, 2012, 14, 7032–7039.
47. N. Wadnerkar and N. J. English, *Comp. Mater. Sci.*, 2013, 74, 33-39.
48. K. E. Kweon and G. S. Hwang, *Phys. Rev. B*, 2013, 87, 205202.
49. J. K. Cooper, S. Gul, F. M. Toma, L. Chen, Y.-S. Liu, J. Guo, J. W. Ager, J. Yano and I. D. Sharp, *J. Phys. Chem. C*, 2015, 119, 2969-2974.
50. H. J. Monkhorst and J. D. Pack, *Phys. Rev. B*, 1976, 13, 5188-5192.
51. A. W. Sleight, H. y. Chen, A. Ferretti and D. E. Cox, *Mater. Res. Bull.*, 1979, 14, 1571-1581.
52. R. Long and N. J. English, *J. Phys. Chem. C*, 2009, 113, 8373-8377.
53. P. Zhou, J. Yu and Y. Wang, *Appl. Catal. B*, 2013, 142, 45-53.
54. W. Luo, J. Wang, X. Zhao, Z. Zhao, Z. Li and Z. Zou, *Phys. Chem. Chem. Phys.*, 2013, 15, 1006-1013.
55. B. N. Cox, M. A. Coulthard and P. Lloyd, *J. Phys. F: Metal Phys.*, 1974, 4, 807-820.
56. X. Ma, Y. Wu, Y. Lu, J. Xu, Y. Wang and Y. Zhu, *J. Phys. Chem. C*, 2011, 115, 16963-16969.
57. K. Ding, B. Chen, Z. Fang, Y. Zhang and Z. Chen, *Phys. Chem. Chem. Phys.*, 2014, 16, 13465-13476.

58. L. Mi, P. Xu, H. Shen, P.-N. Wang and W. Shen, *Appl. Phys. Lett.*, 2007, 90, 171909.
59. M. Li, J. Zhang and Y. Zhang, *Chem. Phys. Lett.*, 2012, 527, 63-66.
60. M. A. Butler, *J. Electrochem. Soc.*, 1978, 125, 228.
61. S. R. Morrison, *Electrochemistry at Semiconductor and Oxidized Metal Electrodes*, Plenum Press, New York, NY, USA, 1980.
62. M. L. Guan, D. K. Ma, S. W. Hu, Y. J. Chen and S. M. Huang, *Inorg. Chem.*, 2011, 50, 800-805.
63. M. V. Putz, N. Russo and E. Sicilia, *Theor. Chem. Acc.*, 2005, 114, 38-45.
64. E. A. Boudreaux, *J. Phys. Chem. A*, 2011, 115, 1713-1720.
65. K. Lai, Y. Zhu, J. Lu, Y. Dai and B. Huang, *Solid State Sci.*, 2013, 24, 79-84.

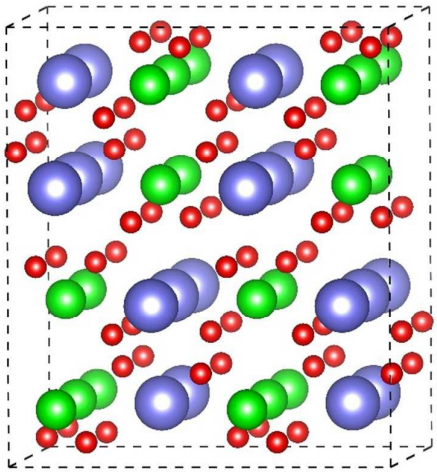

Fig. 1 (color online) The 2 × 2 × 1 supercell of $BiVO_4$, which contains 16 bismuth or vanadium atoms and 64 oxygen atoms. The light blue, green, and red spheres represent Bi, V, and O atoms, respectively.

Table. 1 Formation energies (eV) for Mo,W mondoped and Mo/W co-doped $BiVO_4$.

Doped $BiVO_4$	O-poor	O-rich
W_{Bi}	6.89	2.39
W_V	2.84	-0.15
Mo_{Bi}	5.31	0.81
Mo_V	2.34	-0.65
W_VMo_{Bi}	8.03	0.53
W_VMo_V	5.20	-0.79
$W_{Bi}Mo_V$	9.11	1.61
$W_{Bi}Mo_{Bi}$	11.75	2.75
Mo/W/Mo	7.61	-1.38
W/Mo/W	8.14	-0.86

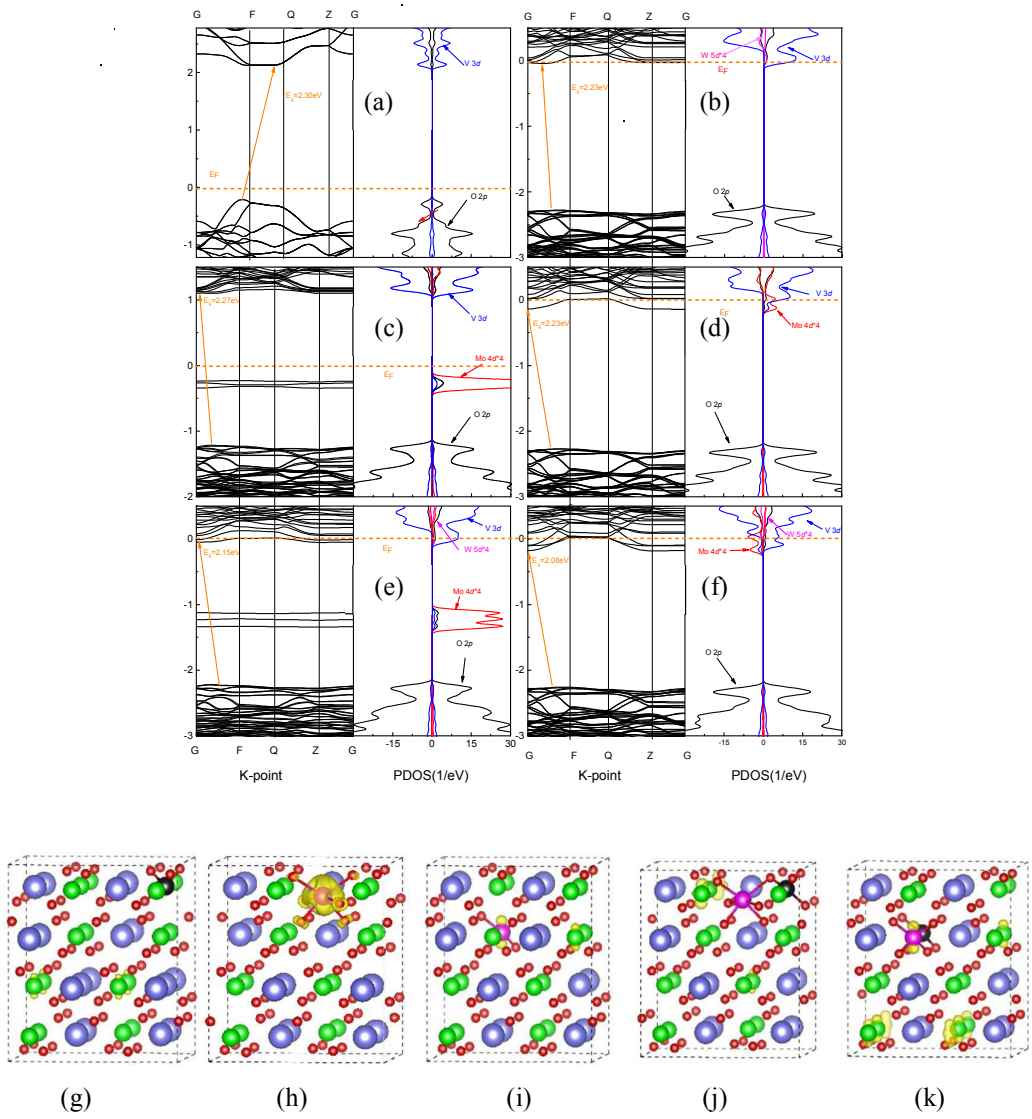

(g) (h) (i) (j) (k)

Fig. 2 (color online) Band structures and projected density of state (PDOS) for pure, Mo,W mondoped and Mo/W codoped $BiVO_4$: (a) pure, (b) W_V, (c) Mo_{Bi}, (d) Mo_V, (e) W_VMo_{Bi} (f) W_VMo_V. (g)-(k) are the band decomposed charge density within the energy range of –0.5 to 0 eV (isosurface values 0.01 e/Å^3) for (b) W_V, (c) Mo_{Bi}, (d) Mo_V, (e) W_VMo_{Bi}, and (f) W_VMo_V. The dashed lines denote the Fermi level at 0 eV. The black lines represent the PDOS of O 2*p*, blue for V 3*d*, red for the quadruplicate of Mo 4*d* and magenta for the quadruplicate of W 5*d*. The light blue, green, red, purple and black spheres represent Bi, V, O, Mo and W atoms, respectively. Only (Mo or W)-O bands and (Mo or W)-V bands are shown. The Mo 4d and W 5d states are multiplied by 4 times to show their distribution clearly.

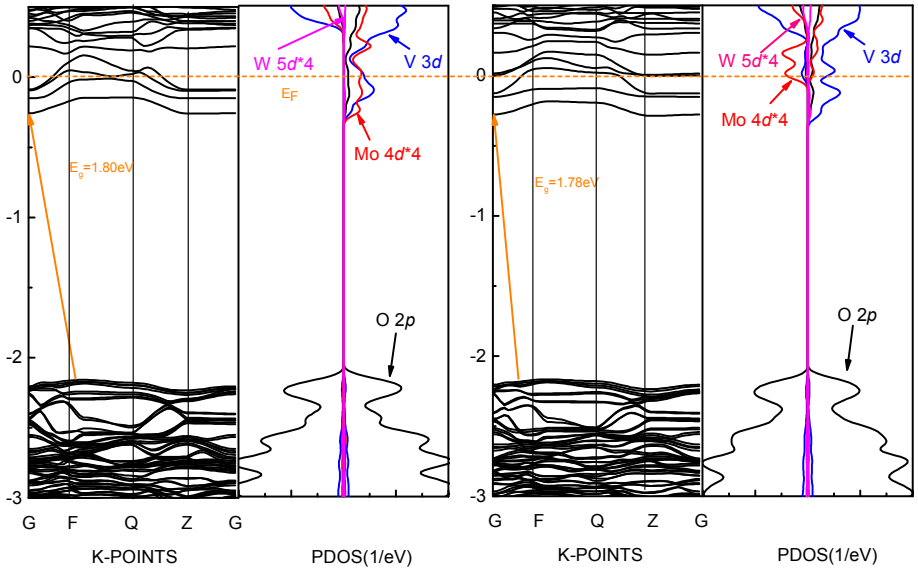

(a) (b)

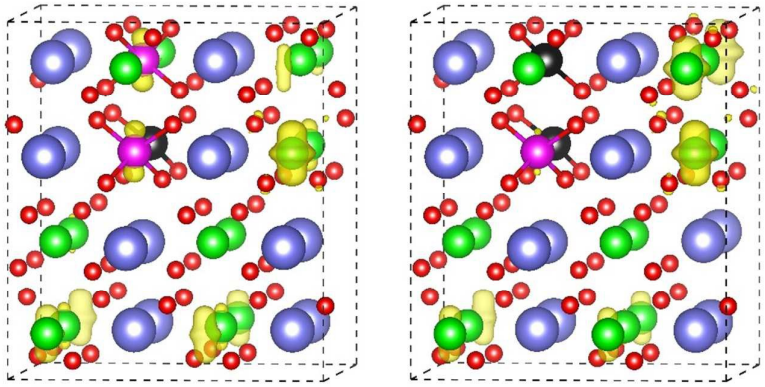

(c) (d)

Fig. 3 (color online) (a)(b)Band structures, projected density of state (PDOS) plots, and (c)(d)the band decomposed charge density within the energy range of–0.5 to 0 eV (isosurface values 0.01 e/Å^3) for Mo/W/Mo-$BiVO_4$ and W/Mo/W-$BiVO_4$. The labeling of the atoms is the same as in Fig. 2. Only (Mo or W)-O bands and (Mo or W)-V bands are shown. The Mo 4d and W 5d states are multiplied by 4 times to show their distribution clearly.

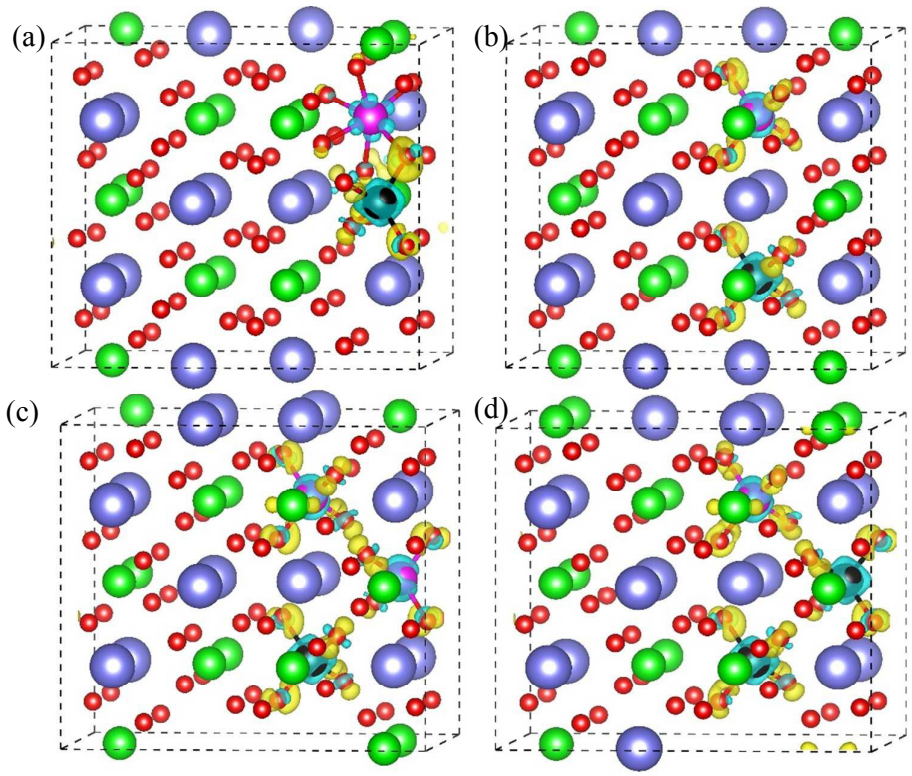

Fig. 4. (Color online) Charge density difference isosurfaces of (a) W_VMo_{Bi} (b) W_VMo_V (c) Mo/W/Mo and (d) W/Mo/W co-doped $BiVO_4$. The cyan region represents charge depletion, and the yellow region represents charge accumulation. The isosurface value is 0.03 e/Å^3. The labeling of the atoms is the same as in Fig. 2. Only (Mo or W)-O bands and (Mo or W)-V bands are shown.

Graphical Abstract